ACS APPLIED MATERIALS & INTERFACES

Research Article

www.acsami.org

Self-Assembled Three-Dimensional Hierarchical Graphene/Polypyrrole Nanotube Hybrid Aerogel and Its Application for Supercapacitors

Shibing Ye and Jiachun Feng*

State Key Laboratory of Molecular Engineering of Polymers, Department of Macromolecular Science and Laboratory of Advanced Materials, Fudan University, Shanghai 200433, China

Supporting Information

ABSTRACT: A three-dimensional hierarchical graphene/polypyrrole aerogel (GPA) has been fabricated using graphene oxide (GO) and already synthesized one-dimensional hollow polypyrrole nanotubes (PNTs) as the feedstock. The amphiphilic GO is helpful in effectively promoting the dispersion of well-defined PNTs to result in a stable, homogeneous GO/PNT complex solution, while the PNTs not only provide a large accessible surface area for fast transport of hydrate ions but also act as spacers to prevent the restacking of graphene sheets. By a simple one-step reduction self-assembly process, hierarchically structured, low-density, highly compressible GPAs are easily obtained, which favorably combine the advantages of graphene and PNTs. The supercapacitor electrodes based on such materials exhibit excellent electrochemical performance, including a high specific capacitance up to 253 F g^{-1}, good rate performance, and outstanding cycle stability. Moreover, this method may be feasible to prepare other graphene-based hybrid aerogels with structure-controllable nanostructures in large scale, thereby holding enormous potential in many application fields.

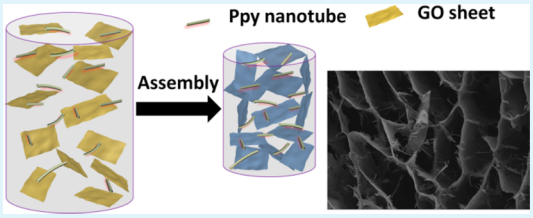

KEYWORDS: *graphene, polypyrrole, aerogel, supercapacitor*

INTRODUCTION

Graphene, a two-dimensional single-layer sheet of sp^2-hybridized conjugated carbon atoms, has attracted persistent attention due to its intriguing electronic, thermal, and mechanical properties.[1−5] However, the transfer of the science into a realistic technology has yet to be completed, and key challenges remain, especially in terms of assembling graphene sheets into macroscopic materials which express the exciting properties of their nanoscale building blocks.[6−8] Graphene aerogel (GA), as one of the most prevailing three-dimensional (3D) macroscopic architectures of graphene, exhibits several attractive features including high porosity, large specific surface area, and high electrical conductivity, thus offering exceptional potential in a variety of sustainable applications, including energy storage, catalysis, and adsorption.[9−17] With the rapid development of above-mentioned technologies, it is urgently required to develop GAs with enhanced mechanical properties or unique functionalities. Recently, graphene-based hybrid aerogels (GHAs) with hierarchical microstructures and various functionalities have been produced by incorporating functional modifiers, such as metal oxide,[18−21] conductive polymers,[22−27] and carbon nanotubes (CNTs),[8,28] into the frameworks of GAs. These nanostructured modifiers not only endow GHAs with novel performance and character[16,20,29,30] but also act as spacers to minimize the agglomeration of graphene sheets.

Polypyrrole (Ppy) is one of the important conductive polymers that are widely used in energy storage systems, biosensors and electronics. Due to its excellent energy storage ability, high conductivity, and strong hydrophobicity, Ppy is considered as one of the most promising functional modifiers for GAs. Shi et al. and other groups have made continuous efforts to fabricate graphene/Ppy aerogels (GPAs), which exhibited high specific surface area, large specific capacitance, and high adsorption capacity.[22−26] Typically, the GPAs were formed via a complicated two-step method, in which pyrrole monomers were first captured by graphene sheets during the hydrothermal self-assembly process, and then an additional polymerization reaction of the pyrrole monomers adsorbed on the graphene sheets should be conducted. This constitutes a major limitation; that is, it is hard to design and control the structure of the Ppy, which significantly impacts the properties of the resulting GPAs, especially for their electrochemical performance. In previous reports, some nanostructures of Ppy, including nanospheres,[31] nanowires,[32,33] and nanotubes[34] have been developed to further enhance the electrochemical activity of Ppy. Among them, the one-dimensional (1D) nanotubes are known for their advantages of the facile electron transportation and the relative larger surface area compared to the nanorods or nanowires.[35] However, to our best knowledge, the fabrication of GPAs with precisely structure-controlled Ppy, including Ppy nanotubes (PNTs), has not been achieved. The main challenge

Received: April 7, 2014
Accepted: May 29, 2014
Published: May 29, 2014

   dx.doi.org/10.1021/am502077p | ACS Appl. Mater. Interfaces 2014, 6, 9671−9679

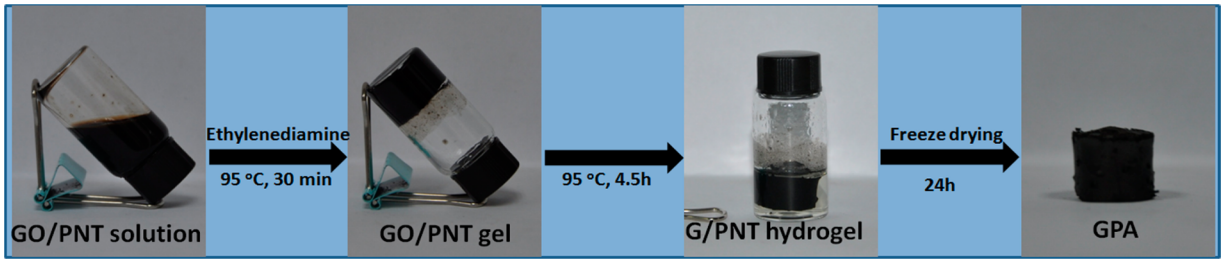

Figure 1. Photographs of time-dependent formation process of GPAs.

is that the strong hydrophobicity and aggregation tendency of Ppy obstacle its uniform dispersion in aqueous solutions.[26]

With the knowledge of surface activity of graphene oxide (GO), we can regard it as an amphiphile with hydrophilic edges and a more hydrophobic basal plane.[36−38] In previous studies,[39−42] some independent groups have realized the dispersion of insoluble CNTs in GO solution by taking advantage of the amphiphilicity of GO. The oxygen-containing groups render GO sheets hydrophilic and highly dispersible in water, whereas the aromatic regions offer active sites to make it possible to interact with CNTs through $\pi-\pi$ interaction. By using this principle, Niu et al. has incorporated various nanomaterials including nanofibers and nanoparticles into GAs by a one-step hydrothermal assembly.[43] Considering that the π-conjugated Ppy exhibits strong $\pi-\pi$ interactions with GO sheets,[34,44] it can be envisioned that the amphiphilic GO sheets have the potential to assist the dispersion of Ppy, especially for PNTs, in aqueous solutions. Once the homogeneous and stable GO/Ppy solution is obtained, it is not a difficult task to synthesize GPAs with precisely structure-controlled Ppy through a simple assembly process of graphene sheets.

Herein, for the first time, we developed a facile one-step approach to the fabrication of GPAs with presynthesized PNTs and GO precursor, which acts as a dispersing agent for PNTs. The 1D, hollow, tubular PNTs were first synthesized and then dispersed in aqueous solutions with the aid of GO sheets. Through a typical self-assembly process during the reduction of GO, GPAs with hierarchical and interconnected structure were obtained. The as-formed GPAs exhibited low density, large specific surface area, and high compressive strength, which is highly required for the porous materials. When working as electrodes for supercapacitors, the GPAs exhibit high specific capacitance of 253 F g^{-1}, good rate performance, and outstanding cycle stability, which is superior to the pure GA and PNTs and mainly attributed to the synergistic effects of both of the individual components. Moreover, the simple and scalable method demonstrated in this work shows great potential in preparing other types of GHAs with desired structures and charming properties.

2. EXPERIMENTAL SECTION

2.1. Preparation of PNTs. The synthesis of PNTs is presented in ref 45: methyl orange (0.784 g) and $FeCl_3$ (3.888 g) were dissolved in deionized water (480 mL), and then, a certain amount of pyrrole (0.84 mL) was added. After stirring for 24 h, the resulting suspension was filtered and washed with deionized water and ethanol several times until filtrate was colorless. Then, the product was freeze-dried for 48 h, followed by vacuum drying at 80 °C for another 8 h.

2.2. Preparation of GPAs. GPAs were prepared according to a modified reduction self-assembly method as reported in previous paper.[9] The formation process of GPAs and the digital images of each steps are illustrated in Figure 1. A uniform GO suspension (2.8 mg mL^{-1}, 10 mL) was first prepared through ultrasonication for 2 h. Then, preweighted PNTs (5.6, 14, and 28 mg) were added and dissolved in above suspensions under vigorous stirring overnight, followed with ultrasonication for 4 h. After mixing with ethylenediamine (20 μL), the GO/PNTs suspensions were transferred into four seal glass vials with an inner diameter of ∼10 mm before reaction at 95 °C. The mixture suspensions turned black and sticky in the first 30 min and finally transformed into graphene/PNT (G/PNT) hydrogels after reaction for another 4.5 h. Before freeze-drying the hydrogels to obtain GPAs, they were dialyzed with ultrapure water for 1 week. According to the feed weight ratio of GO to PNT, the resulting aerogels were denoted as GPA51, GPA21, and GPA11, respectively. For comparison, the pure GA was also prepared under the similar conditions, without using PNT as a raw material.

2.3. Characterization and Tests. The morphology of PNTs and aerogels was characterized by a Zeiss Ultra 55 field-emission scanning electron microscopy (SEM) at an operating voltage of 5 kV. Transmission electron microscopy (TEM) images were acquired on a JEOL JEM2100F microscope at 200 kV. Fourier transform infrared (FTIR) spectra were recorded on a Nicolet Nexus 470 spectrometer. The elementary composition was determined using a Thermo ESCALAB 250XI X-ray photoelectron spectroscopy (XPS). Wide-angle X-ray diffraction (XRD) analyses were carried out on a PANalytical X'pert PRO X-ray diffractometer with Cu Kα radiation. Raman spectra were collected using a Renishaw inVia Reflex micro-Raman spectrometer with 633 nm laser excitation. The specific surface area was measured from the N_2 adsorption−desorption isotherms on the ASAP2020 Brunauer−Emmett−Teller (BET) apparatus. The mechanical properties of GPAs were tested using a SANS CMT-6503 universal testing machine, fitted with a 50 N load cell. For the compression tests, the cylindrical samples were placed between the self-leveling plates and compressed at a rate of 1 mm/min until a constant compression ratio of 70%. Electrochemical analyses were performed using a three-electrode system equipped with a Hg/HgO reference electrode and a platinum counter electrode. Working electrodes were prepared by pasting a mixture of GA, PNTs, and GPAs (80 wt %) with conductive black (10 wt %) and binding material (10 wt %) onto stainless steel mesh with a mass of ∼2 mg. All of the electrochemical measurements including cyclic voltammetry (CV), galvanostatic charge−discharge (GCD), and electrochemical impedance spectroscopy (EIS) were carried out using an electrochemical workstation CHI660D in a H_2SO_4 electrolyte (1 M). The specific capacitance (F g^{-1}) was obtained from the discharge process according to the following equation:

$$Cs = \frac{I \times \Delta t}{m \times \Delta V}$$

where I is the current loaded (A), Δt is the discharge time (s), ΔV is the potential change during the discharge process, and m is the mass of active material (g).

3. RESULTS AND DISCUSSION

3.1. Characterization of PNTs. Before the assembly of GPAs, PNT is synthesized by a reactive self-degraded template method according to previous process.[45] The FTIR spectrum of

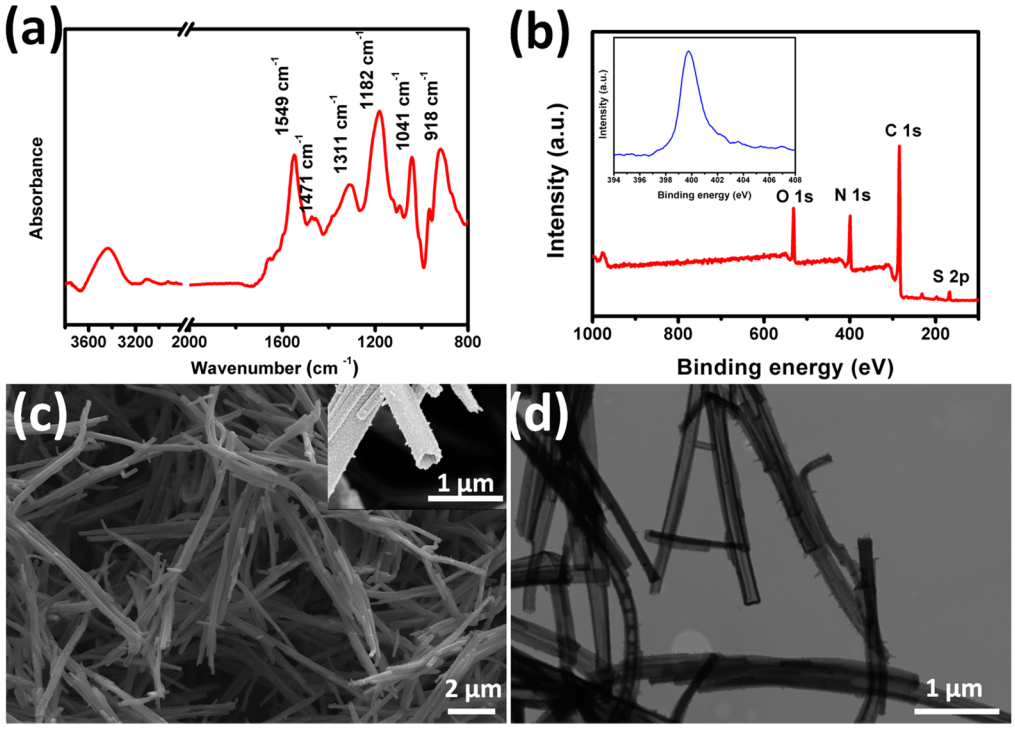

Figure 2. FTIR spectrum (a), XPS spectrum (b), SEM image (c), and TEM image (d) of the as-prepared PNTs. The inset in part b is N 1s spectrum of PNTs, and the inset in part c is an enlarged view of an individual PNT.

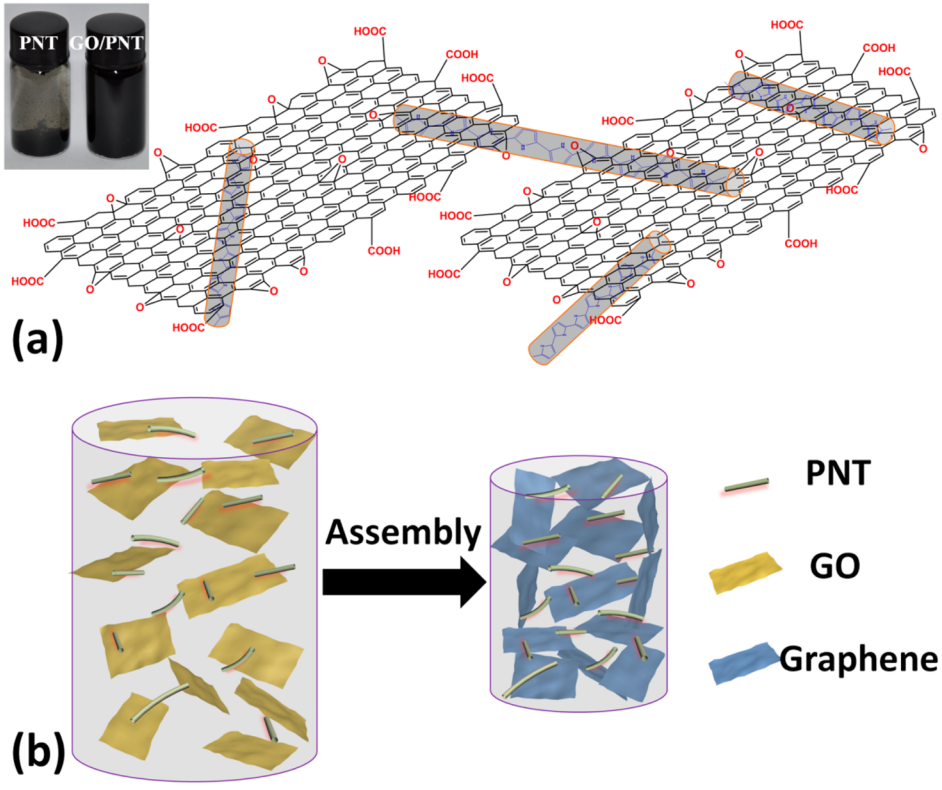

Figure 3. Schematic illustration for the interactions between GO sheets and PNTs (a) and the formation process of GPAs (b).

PNTs (Figure 2a) presents characteristic Ppy peaks located at 1549 and 1471 cm^{-1}, due to the symmetric and antisymmetric ring-stretching modes, respectively. The peaks at 1040 and 1311 cm^{-1} should be attributed to C−H deformation vibrations and C−N stretching vibrations, respectively.[46] The two strong peaks near 1182 and 918 cm^{-1} suggest the doping state of Ppy and a broad band at 3000−3500 cm^{-1} arises from N−H and C−H stretching vibrations.[47] XPS was also used to further ascertain the chemical composition of PNTs. As shown in Figure 2b, the PNTs mainly contain C (71.7%), N (16.2%), O

dx.doi.org/10.1021/am502077p | ACS Appl. Mater. Interfaces 2014, 6, 9671−9679

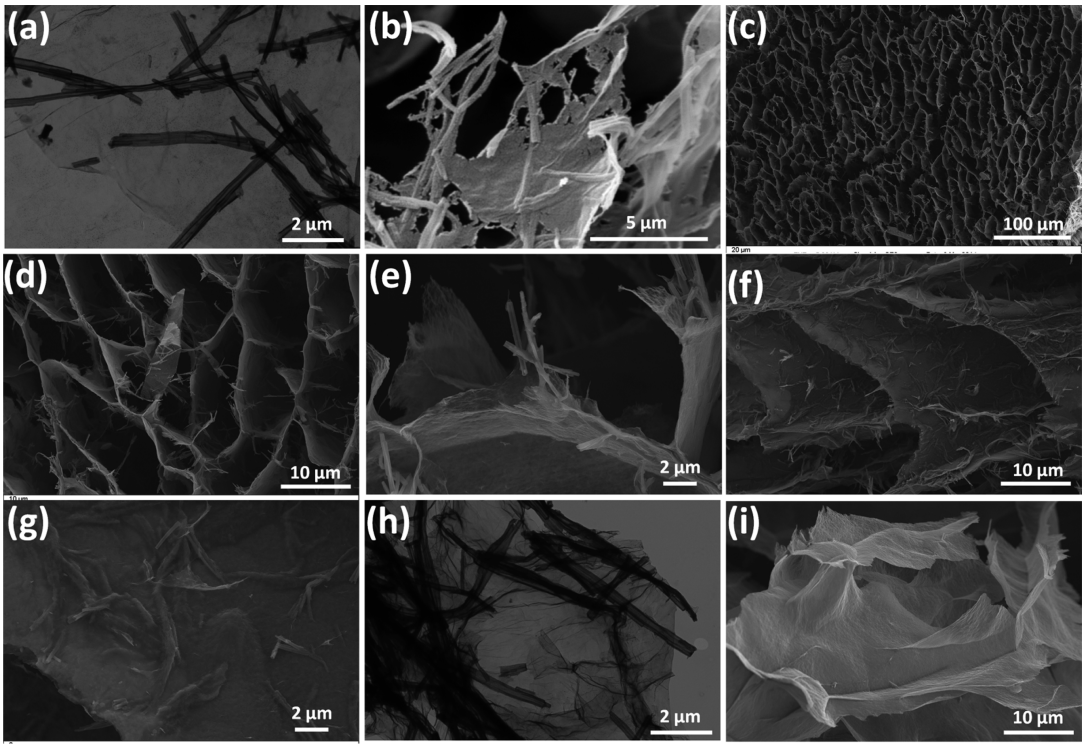

Figure 4. TEM (a) and SEM (b) images of GO/PNT complex, SEM images with different magnifications (c–g), TEM image (h) of the GPA21, and SEM image (i) of pure GA.

(10.0%), and S (2.1%). The presence of a small amount sulfur may originate from the residue of methyl orange template, which has doped into the Ppy polymers.[45] It is seen in the N 1s spectrum that the single peak at ~399.7 eV corresponds to N atoms within the pentagonal ring of the Ppy.[48] Based on the above results, we believe the nanostructures are indeed Ppy and in the doping states.

SEM image in Figure 2c shows that the as-prepared PNTs have high-quality tubular morphology with diameters of 60–80 nm and lengths of 5–10 μm. An enlarged image in the inset reveals the hollow structure of PNTs. TEM image further confirms that PNT is a 1D nanotube with an internal cavity (Figure 2d). It can be obviously seen that bundles of more than five individual nanotubes are formed, which should be induced by the $\pi-\pi$ interaction of partial PPy chains. Similar to the CNTs, this aggregation will lead to the insolubility of pure PNTs in water, which greatly limits their integration in potential applications.

3.2. Formation, Morphology, Structure, and Mechanical Properties of GPAs. The homogeneous dispersion of PNTs in GO solutions is a crucial step in determining the macroscopic architecture of GPAs. The hydrophobicity and aggregation of PNTs make it difficult to form stable PNT aqueous suspensions, and serious precipitation always occurs even after a long time ultrasonication (inset of Figure 3a). Inspired by the surfactant behaviors of GO for CNTs, herein, we develop GO as a molecular dispersing agent to help the dispersion of PNTs. During the dispersion process, PNTs agglomerates are first disassembled into smaller bundles or individual tubes with the assist of ultrasonication. Amounts of GO sheets distribute around these PNTs and interact with the sidewalls of PNTs through $\pi-\pi$ interaction. As shown by the schematic illustration in Figure 3a, in the mixed suspensions, GO sheets are able to capture PNTs with multiple adhesion sites by π-stacking interaction between the delocalized electrons in both the aromatic regions of GO sheets and PNTs. As a result, GO sheets support and prevent the insoluble PNTs from precipitation, forming a stable suspension (inset of Figure 3a). Similar to the self-assembly of other GHAs,[21,28,30,43] the formation of GPAs is easy to understand, which is simply depicted in Figure 3b. The PNTs homogeneously dispersed in GO aqueous suspension were embedded into the graphene network to form a 3D GPA during the reduction and self-assembly of GO sheets. It is generally recognized that the formation of the 3D graphene networks is driven by various interactions including the $\pi-\pi$ interaction, hydrogen bonding, and the physical entanglement of the graphene sheets.

In order to examine the dispersion of PNTs in the mixed GO/PNT suspension, the observations of both SEM and TEM were carried out. TEM image of the GO/PNT complex displays that the single GO sheet was bestrewed with dozens of PNTs (Figure 4a). By freeze-drying the GO/PNT suspension, a 3D aerogel of GO/PNT was obtained, which can visually reveal the morphology of GO sheets and PNTs. The GO/PNT aerogel exhibits an amorphous, interconnected, porous 3D framework of crinkly GO sheets and randomly oriented PNTs with continuous macropores ranged from hundreds of nanometers to tens of micrometers. Detailed observation in Figure 4b presents multiform interconnections of GO sheets and PNTs: most PNTs are homogeneously and densely attached on the surface of GO sheets through π-stacking interaction, some bridge the separated GO sheets or the defects in single GO sheet. These results indicate GO sheets can assist the dispersion and stabilization of PNTs, which effectively overcomes the aggregation problem of PNTs in water.

Here, we take GPA21 as an example to demonstrate the morphology, structure, properties, and applications of GPAs. Figure 4c–g shows the SEM images of a cross-section of the as-

prepared GPA21. As expected, it exhibits a honeycomb-like cellular structure with the cell dimension in the order of tens of micrometers and the cell walls slightly corrugated (Figure 4c), similar to those of previous neat graphene aerogels.[9,10] An enlarged view of the cross-sectional portion of GPA21 shows that PNTs are uniformly grown on the cell walls of the honeycomb (Figure 4d). Zooming in on a single sheet reveals PNTs can firmly anchor to the edges of graphene sheets or connect the adjacent individual graphene sheets (Figure 4e). From the longitudinal view of the GPA21, the interlamellar spaces of the adjacent walls are homogeneously covered with PNTs (Figure 4f). In fact, the cell walls indicate a multilayered structure, where the PNTs are tightly sandwiched between graphene layers (Figure 4g). TEM image also displays the homogeneous dispersion of PNTs on the graphene sheets (Figure 4h), even after intense ultrasonication, which further confirms the strong interaction between PNTs and graphene sheets. This unique structure will prevent the restacking of graphene sheets to a certain extent, which can provide a large accessible surface area for fast transport of hydrate ions. On the contrary, a serious restacking of graphene sheets is inevitable for pure GA. As shown in Figure 4i, the surfaces of graphene sheets are smooth and flat, which results in highly stacked graphene layers that construct the cell walls of GA.

Raman spectroscopy was used to further study the structure of GPAs and the interaction between PNTs and graphene sheets. As presented in Figure 5, two representative bands at

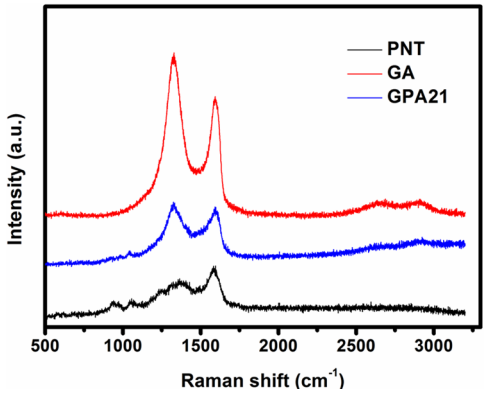

Figure 5. Raman spectra of PNT, GA, and GPA21.

1328 (D band) and 1600 cm^{-1} (G band), and a weaker 2D band are observed for the pure GA, which suggest the reduction of GO to graphene.[25] The Raman spectrum of PNT includes two wide bands at 1360 and 1588 cm^{-1} due to the C=C backbone stretching and the ring-stretching mode, respectively, and the other prominent peaks at 937, 1039, and 1232 cm^{-1}, which are the characteristic peaks of Ppy.[23,49] For the GPA21, apart from the typical D and G bands of graphene, it also contains a series of peaks consistent with those of PNTs. Combined with the FTIR spectra of PNT and GPAs (Supporting Information Figure S1), these results evidence the successful construction of graphene-PNT architecture. Moreover, the broad D band with weak intensity would be attributed to the interaction between PNTs and graphene sheets.[44,49] The intensity ratios of D and G bands (I_D/I_G) were calculated to be 1.31 and 1.11 for GA and GPA21, respectively, higher than 0.93 for GO (Supporting Information Figure S2), indicating the reduction of GO into graphene during the assembly process.

The 3D, porous structure of GPA, together with the hollow PNTs, makes it have the potential to be a kind of ultralight materials. Pure GA exhibits a low density of 0.04 g cm^{-3}, and this value could be tuned by varying the concentration of GO solution. With the incorporation of PNTs, the bulk densities of aerogels increase slightly, are 0.064, 0.084, and 0.095 g cm^{-3} for GPA51, GPA21, and GPA11, respectively (Figure 6). The BET

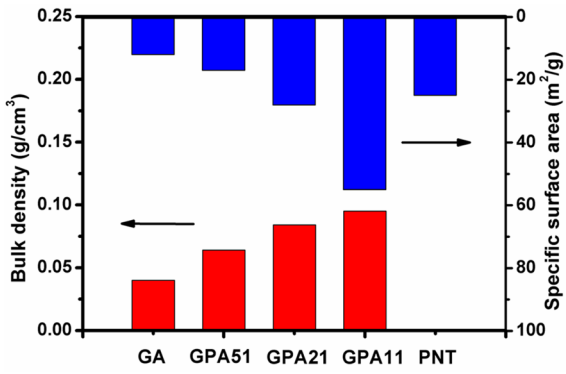

Figure 6. Density (bottom) and BET specific surface area (top) of GA and GPAs.

specific surface area of the aerogels and PNTs were investigated by nitrogen isothermal adsorption. As shown in Figure 6, the BET specific surface area is smaller than the values of GAs prepared by other methods.[15,17] This may be caused by the following factors: First, the reduction degree of GO is limited because the aerogels did not undergo further reduction such as thermal reduction or microwave irradiation. Furthermore, the large pore sizes of GA and GPAs beyond the range accessible to gas adsorption and freeze-dried aerogels would have less available surfaces because of their slight volume shrinkages.[50] However, the incomplete values still can reflect the tendency of the change in BET specific surface area, which are 17, 28, and 55 $m^2\ g^{-1}$ for GPA51, GPA21, and GPA11, respectively. This value is higher than that of pure GA (12 $m^2\ g^{-1}$), and increases as the content of PNT increases. Given that pure PNT only has a small BET specific surface area of 24 $m^2\ g^{-1}$, to be sure, the addition of PNT increases the BET specific surface area of GPAs, indicating that the existence of PNT can prevent the restacking of graphene sheets.

Unexpectedly, the as-formed GPAs exhibit excellent mechanical properties, which certainly expands their potential application fields. As displayed in Figure 7a, pure GA can be easily squeezed into a pellet under pressure, although it recovers from strain as high as nearly 50%. Conversely, the GPAs exhibit more satisfactory mechanical strength and press-resistance. For example, a dried GPA21 monolith (~20 mg) can support at over 5000 times of its own weight without collapsing (Figure 7b). The mechanical property of the aerogels was assessed by measuring the compressive stress−strain curves (Figure 7c). Both GA and GPAs manifest three regimes of deformation in the loading stress−strain curve, including nearly linear elastic regime (corresponding to bending of the cell walls); relatively flat stress plateau (corresponding to elastic buckling of cell walls); and abrupt stress increasing regime (corresponding to densification of cells).[10] GPA21 possesses a compressive strength of ~0.35 MPa at 70% compression strain, which is 7-fold higher than that of pure GA (0.05 MPa). The average compressive strengths for each sample are given in the

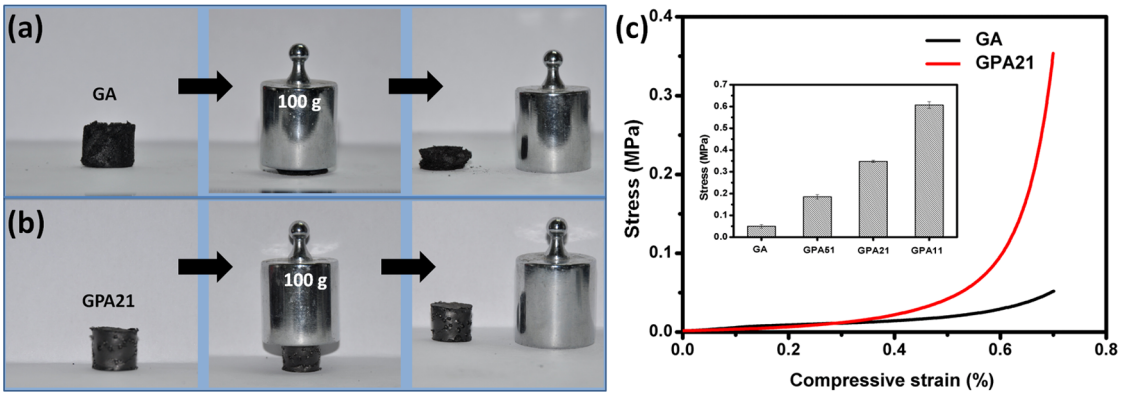

Figure 7. Digital images showing compressibility of pure GA (a) and GPA21 (b), and the compressive stress−strain curves of GA and GPA21 at the maximum strain of 70% (c), inset is the average compressive strength of GA and GPAs.

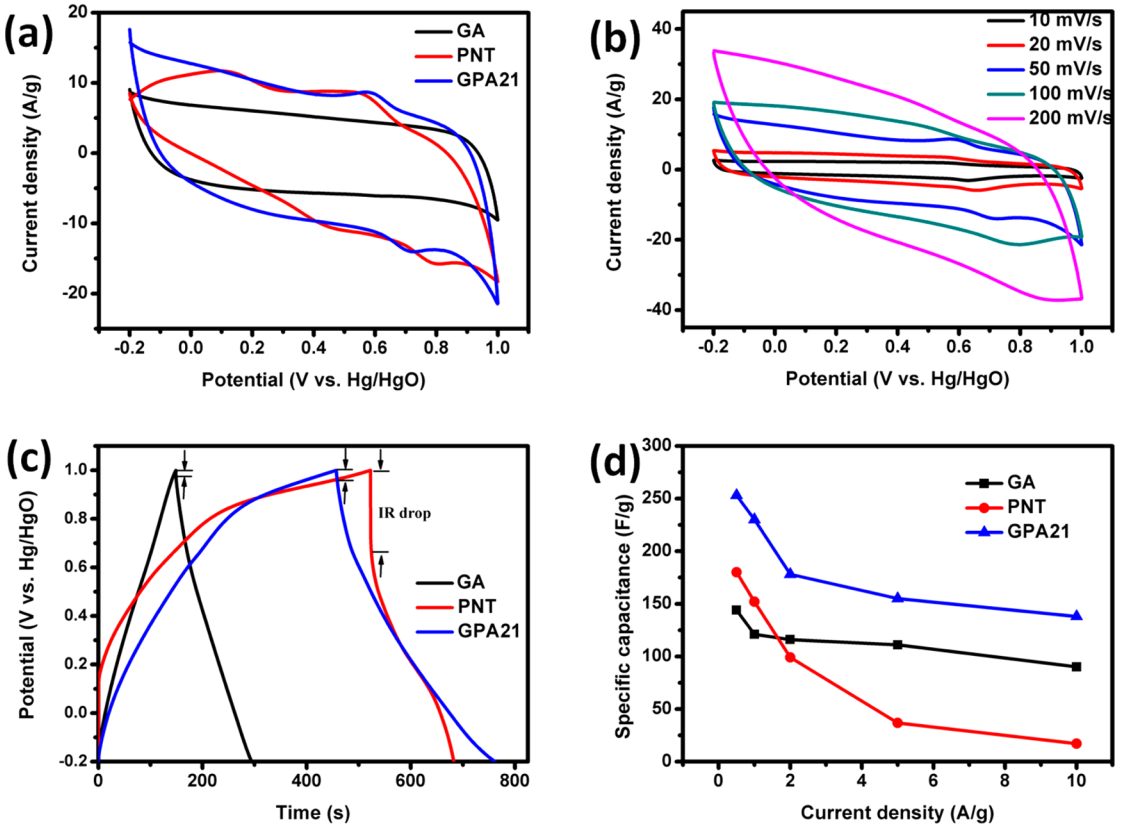

Figure 8. (a) CV curves of PNTs, GA, and GPA21 at 50 mV s^{-1}. (b) CV curves of GPA21 at different scan rates of 10, 20, 50, 100, and 200 mV s^{-1}. (c) GCD curves of PNTs, GA, and GPA21 at 1 A g^{-1}. (d) Specific capacitance of PNTs, GA, and GPA21 as a function of current density.

inset of Figure 7c, with the increase of the mass ratio of PNT to GO from 1:5 to 1:2 and 1:1, the obtained corresponding aerogels, GPA51, GPA21, and GPA11, demonstrate the enhanced compressive strengths of 0.19, 0.35, and 0.61 MPa. This increase should be attributed to the enhancement effect of PNTs, as well as the strong interfacial interactions between graphene sheets and PNTs.

3.3. Electrochemical Performance of Supercapacitors Based on GPAs. It is important to emphasize that the 1D conductive PNTs not only prevent the aggregation and restacking of graphene sheets in some extent but also locally improve the conductivity of the aerogels by providing conductive pathways through defects of graphene and bridging the neighboring graphene sheets.[51] Additionally, the incorporation of conductive polymers into the GAs can effectively improve their energy density due to the pseudocapacitance originating from conducting polymers.[43] Both of the two effects indicate that GPA has great potential as an efficient electrode material for supercapacitors. Herein, we investigate their electrochemical performance in 1 M H_2SO_4 aqueous solution using a three-electrode system. The CV curves measured at a scan rate of 50 mV s^{-1} within a potential window of −0.2 to 1.0 V vs a Hg/HgO electrode are shown in Figure 8a. It can be seen that the CV curve of pure GA shows approximately rectangular shape which is characteristic for an electrical double layer (EDL) capacitor. Whereas, the CV curve of PNTs clearly exhibits a pair of redox peaks, which are an indication of typical pseudocapacitance of PNTs. As for GPA21, its CV curve shows

dx.doi.org/10.1021/am502077p | ACS Appl. Mater. Interfaces 2014, 6, 9671−9679

some Faradaic humps and is somehow distorted, indicating that the specific capacitance results from the combination of EDL capacitance and pseudocapacitance, which are attributable to the graphene and PNTs, respectively.[31] Figure 8b shows the CV curves of GPA21 at scan rates ranging from 10 to 200 mV s^{-1}. When the scan rate increases from 10 up to 200 mV s^{-1}, the CV curve still keep a quasi-rectangular shape with small distortion, while the current density of the CV curves is directly proportional to the scan rate, which implies that the GPA21 possess better rate capabilities and lower internal resistances than GA and PNTs, whose CV curves can be found in Supporting Information Figure S3.

Compared with the linear and symmetric GCD curve of GA-based supercapacitor, the GCD curves of PNT and GPA21 have asymmetrical triangle shapes, indicating the presence of pseudocapacitance (Figure 8c). It is noted that there is a significant IR drop in the GCD curve of PNTs, due to the large internal resistance of PNTs. In the GCD curves of GA and GPA21, the IR drop is almost negligible and much smaller than that of PNTs. From the slope of the GCD curves, the specific capacitance is calculated to be 144, 180, and 253 F g^{-1} at the current density of 0.5 A g^{-1} for GA, PNTs, and GPA21, respectively. Figure 8d shows the specific capacitance of the electrode materials as a function of discharge current density. The specific capacitance of GPA21 still remains as high as 138 F g^{-1} even at a high current density of 10 A g^{-1}, indicating an excellent rate capability, which is much better than PNTs. These results suggest that the incorporation of PNTs into GA can greatly improve the capacitance of the composites and indicate that hybridization of PNTs with graphene may allow comprehensive utilization of the EDL capacitance of graphene and the pseudocapacitance of PNTs to produce synergistic effects.

EIS analysis is another principal method for examining the fundamental behavior of electrode materials.[52] The resulting Nyquist plots in Figure 9 further confirm the favorable performance of GPA electrodes. In the high-frequency region, the real axis intercept represents the equivalent series resistance (ESR), which is the sum of the resistance of the electrolyte solution, the intrinsic resistance of the active material, and the contact resistance of the interface active material/current collector.[53] The ESR values of GA, PNT, and GPA21 are determined to be 0.65, 0.53, and 0.36 Ohm, respectively, indicating that the resistance has been efficiently decreased by hybriding graphene and PNTs. The projected length of the Warburg-type line (the slope of 45° portion of the curve) on the real axis characterizes the ion diffusion process from solution into the intermediate-frequency region.[54] As shown in the inset of Figure 9, The Warburg curve of GPA21 is as short as that of pure GA and much shorter than that of PNTs, suggesting low electronic resistance and fast ion diffusion in GPA21. The low-frequency region of the Nyquist plot is a vertical line for an ideal electrode material.[55] Both GA and GPA21 exhibit relatively vertical lines compared with PNTs, which suggest they behave more closely to an ideal capacitor.

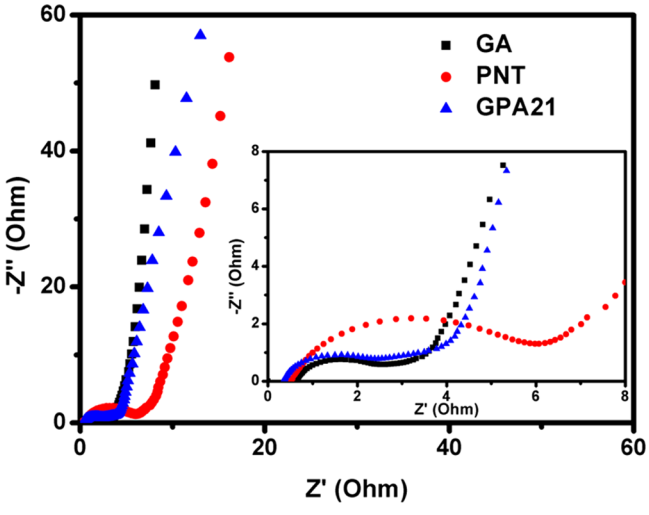

Figure 9. Nyquist plots of PNTs, GA, and GPA21, inset is the expanded high-frequency region of the plots.

Stability over repeated charge−discharge cycling is critical for supercapacitors in practice. As we know that Ppy generally shows poor cycle stability due to the pseudocapacitance behavior. As expected, when the PNTs are embedded into GAs, the resultant GPA21 shows good cycle performance. As shown in Figure 10, the specific capacitance of PNTs drops

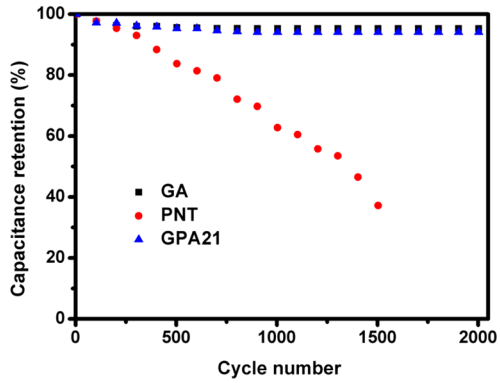

Figure 10. Cycle life of PNTs, GA, and GPA21 measured at a current density of 10 A g^{-1}.

significantly with ~70% decrease after 1500 cycles, which could be ascribed to the unstable carbon skeleton of Ppy during charge−discharge process.[56,57] Whereas, the capacitance retentions for GA and GPA21 can reach 95 and 93% after 2000 cycles, respectively. The graphene sheets provide a robust support for the PNTs, thus enhancing the mechanical strength of the composites and preventing the PNTs from swelling and shrinking during the long-term cycling. Therefore, the GPA21 exhibits a better stability compared with the pristine PNTs.

4. CONCLUSIONS

In summary, a 3D hierarchical graphene/polypyrrole hybrid aerogel was fabricated using GO sheets and already synthesized one-dimensional hollow PNTs as the feedstock, which has realized the fabrication of GPAs with precisely structure-controlled Ppy nanostructures. One-dimensional, hollow, tubular PNTs were first synthesized and then dispersed uniformly in water with the assist of amphiphilic GO sheets, which act as a dispersing agent. During a typical reduction process, GO sheets were self-assembled together to form a network, in which the PNTs were simultaneously captured into the graphene network. The as-formed GPAs exhibit hierarchical structure, low density, and excellent mechanical property, and show higher specific surface area than pure GA. As the electrode materials for supercapacitor, the GPAs manifest a

high specific capacitance up to 253 F g^{-1}, good rate performance, and outstanding cycle stability, which should be attributed to the synergistic effects of graphene and PNTs. On the basis of above results, the simple method demonstrated in this study shows great potential in preparing other GHAs with desired structures and charming properties.

■ ASSOCIATED CONTENT

Supporting Information

FTIR spectra of GO and GPA21, Raman spectrum of GO, and CV curves of GA and PNT at different scan rates. This material is available free of charge via the Internet at http://pubs.acs.org.

■ AUTHOR INFORMATION

Corresponding Author

*Tel: 86 21 6564 3735. Fax: +86 21 6564 0293. Email: jcfeng@fudan.edu.cn.

Notes

The authors declare no competing financial interest.

■ ACKNOWLEDGMENTS

This work was financially supported by the Natural Science Foundation of China (21174032 and 51373042) and National Basic Research Program of China (2011CB605704).

■ REFERENCES

(1) Pei, S.; Cheng, H.-M. The Reduction of Graphene Oxide. *Carbon* **2012**, *50*, 3210−3228.
(2) Geim, A. K. Graphene: Status and Prospects. *Science* **2009**, *324*, 1530−1534.
(3) Zhu, Y.; Murali, S.; Cai, W.; Li, X.; Suk, J. W.; Potts, J. R.; Ruoff, R. S. Graphene and Graphene Oxide: Synthesis, Properties, and Applications. *Adv. Mater.* **2010**, *22*, 3906−3924.
(4) Novoselov, K.; Geim, A. K.; Morozov, S.; Jiang, D.; Grigorieva, M. K. I.; Dubonos, S.; Firsov, A. Two-Dimensional Gas of Massless Dirac Fermions in Graphene. *Nature* **2005**, *438*, 197−200.
(5) Cao, Y.; Zhang, J.; Feng, J.; Wu, P. Compatibilization of Immiscible Polymer Blends using Graphene Oxide Sheets. *ACS Nano* **2011**, *5*, 5920−5927.
(6) Xu, Z.; Gao, C. Graphene Chiral Liquid Crystals and Macroscopic Assembled Fibres. *Nat. Commun.* **2011**, *2*, 571.
(7) Tian, Y.; Cao, Y.; Wang, Y.; Yang, W.; Feng, J. Realizing Ultrahigh Modulus and High Strength of Macroscopic Graphene Oxide Papers Through Crosslinking of Mussel-Inspired Polymers. *Adv. Mater.* **2013**, *25*, 2980−2983.
(8) Sun, H.; Xu, Z.; Gao, C. Multifunctional, Ultra-Flyweight, Synergistically Assembled Carbon Aerogels. *Adv. Mater.* **2013**, *25*, 2554−2560.
(9) Hu, H.; Zhao, Z.; Wan, W.; Gogotsi, Y.; Qiu, J. Ultralight and Highly Compressible Graphene Aerogels. *Adv. Mater.* **2013**, *25*, 2219−2223.
(10) Qiu, L.; Liu, J. Z.; Chang, S. L.; Wu, Y.; Li, D. Biomimetic Superelastic Graphene-based Cellular Monoliths. *Nat. Commun.* **2012**, *3*, 1241.
(11) Chen, P.; Yang, J.-J.; Li, S.-S.; Wang, Z.; Xiao, T.-Y.; Qian, Y.-H.; Yu, S.-H. Hydrothermal Synthesis of Macroscopic Nitrogen-Doped Graphene Hydrogels for Ultrafast Supercapacitor. *Nano Energy* **2013**, *2*, 249−256.
(12) Xu, Z.; Zhang, Y.; Li, P.; Gao, C. Strong, Conductive, Lightweight, Neat Graphene Aerogel Fibers with Aligned Pores. *ACS Nano* **2012**, *6*, 7103−7113.
(13) Xu, Y.; Sheng, K.; Li, C.; Shi, G. Self-Assembled Graphene Hydrogel via A One-Step Hydrothermal Process. *ACS Nano* **2010**, *4*, 4324−4330.
(14) Sun, Y.; Wu, Q.; Shi, G. Graphene Based New Energy Materials. *Energy Environ. Sci.* **2011**, *4*, 1113−1132.
(15) Worsley, M. A.; Pauzauskie, P. J.; Olson, T. Y.; Biener, J.; Satcher, J. H., Jr; Baumann, T. F. Synthesis of Graphene Aerogel with High Electrical Conductivity. *J. Am. Chem. Soc.* **2010**, *132*, 14067−14069.
(16) Zhao, Y.; Hu, C.; Hu, Y.; Cheng, H.; Shi, G.; Qu, L. A Versatile, Ultralight, Nitrogen-Doped Graphene Framework. *Angew. Chem., Int. Ed.* **2012**, *124*, 11533−11537.
(17) Zhang, X.; Sui, Z.; Xu, B.; Yue, S.; Luo, Y.; Zhan, W.; Liu, B. Mechanically Strong and Highly Conductive Graphene Aerogel and Its Use as Electrodes for Electrochemical Power Sources. *J. Mater. Chem.* **2011**, *21*, 6494−6497.
(18) Chen, L.; Wei, B.; Zhang, X.; Li, C. Bifunctional Graphene/γ-Fe_2O_3 Hybrid Aerogels with Double Nanocrystalline Networks for Enzyme Immobilization. *Small* **2013**, *9*, 2331−2340.
(19) Cong, H.-P.; Ren, X.-C.; Wang, P.; Yu, S.-H. Macroscopic Multifunctional Graphene-Based Hydrogels and Aerogels by a Metal Ion Induced Self-Assembly Process. *ACS Nano* **2012**, *6*, 2693−2703.
(20) Wu, Z.-S.; Yang, S.; Sun, Y.; Parvez, K.; Feng, X.; Müllen, K. 3D Nitrogen-Doped Graphene Aerogel-Supported Fe_3O_4 Nanoparticles as Efficient Electrocatalysts for the Oxygen Reduction Reaction. *J. Am. Chem. Soc.* **2012**, *134*, 9082−9085.
(21) Chen, W.; Li, S.; Chen, C.; Yan, L. Self-Assembly and Embedding of Nanoparticles by In Situ Reduced Graphene for Preparation of a 3D Graphene/Nanoparticle Aerogel. *Adv. Mater.* **2011**, *23*, 5679−5683.
(22) Zhou, H.; Ni, T.; Qing, X.; Yue, X.; Li, G.; Lu, Y. One-Step Construction of Graphene−Polypyrrole Hydrogels and Their Superior Electrochemical Performance. *RSC Adv.* **2014**, *4*, 4134−4139.
(23) Zhao, Y.; Liu, J.; Hu, Y.; Cheng, H.; Hu, C.; Jiang, C.; Jiang, L.; Cao, A.; Qu, L. Highly Compression-Tolerant Supercapacitor Based on Polypyrrole-Mediated Graphene Foam Electrodes. *Adv. Mater.* **2013**, *25*, 591−595.
(24) Bai, H.; Sheng, K.; Zhang, P.; Li, C.; Shi, G. Graphene Oxide/Conducting Polymer Composite Hydrogels. *J. Mater. Chem.* **2011**, *21*, 18653−18658.
(25) Liu, J.; Wang, Z.; Zhao, Y.; Cheng, H.; Hu, C.; Jiang, L.; Qu, L. Three-Dimensional Graphene−Polypyrrole Hybrid Electrochemical Actuator. *Nanoscale* **2012**, *4*, 7563−7568.
(26) Li, H.; Liu, L.; Yang, F. Covalent Assembly of 3D Graphene/Polypyrrole Foams for Oil Spill Cleanup. *J. Mater. Chem. A* **2013**, *1*, 3446−3453.
(27) Ye, S.; Feng, J.; Wu, P. Highly Elastic Graphene Oxide-Epoxy Composite Aerogels via Simple Freeze-Drying and Subsequent Routine Curing. *J. Mater. Chem. A* **2013**, *1*, 3495−3502.
(28) Sui, Z.; Meng, Q.; Zhang, X.; Ma, R.; Cao, B. Green Synthesis of Carbon Nanotube−Graphene Hybrid Aerogels and Their Use as Versatile Agents for Water Purification. *J. Mater. Chem.* **2012**, *22*, 8767−8771.
(29) Wu, Z.-S.; Ren, W.; Wang, D.-W.; Li, F.; Liu, B.; Cheng, H.-M. High-Energy MnO_2 Nanowire/Graphene and Graphene Asymmetric Electrochemical Capacitors. *ACS Nano* **2010**, *4*, 5835−5842.
(30) Yin, H.; Zhao, S.; Wan, J.; Tang, H.; Chang, L.; He, L.; Zhao, H.; Gao, Y.; Tang, Z. Three-Dimensional Graphene/Metal Oxide Nanoparticle Hybrids for High-Performance Capacitive Deionization of Saline Water. *Adv. Mater.* **2013**, *25*, 6270−6276.
(31) Zhang, J.; Yu, Y.; Liu, L.; Wu, Y. Graphene-Hollow PPy Sphere 3D-Nanoarchitecture with Enhanced Electrochemical Performance. *Nanoscale* **2013**, *5*, 3052−3057.
(32) Biswas, S.; Drzal, L. T. Multilayered Nanoarchitecture of Graphene Nanosheets and Polypyrrole Nanowires for High Performance Supercapacitor Electrodes. *Chem. Mater.* **2010**, *22*, 5667−5671.
(33) Zhang, L. L.; Zhao, S.; Tian, X. N.; Zhao, X. Layered Graphene Oxide Nanostructures with Sandwiched Conducting Polymers as Supercapacitor Electrodes. *Langmuir* **2010**, *26*, 17624−17628.
(34) Liu, J.; An, J.; Ma, Y.; Li, M.; Ma, R. Synthesis of A Graphene-Polypyrrole Nanotube Composite and Its Application in Supercapacitor Electrode. *J. Electrochem. Soc.* **2012**, *159*, A828−A833.
(35) Huang, T.-Y.; Kung, C.-W.; Wei, H.-Y.; Boopathi, K. M.; Chu, C. W.; Ho, K.-C. A High Performance Electrochemical Sensor for

Acetaminophen Based on rGO/PEDOT Nanotube Composite Modified Electrode. *J. Mater. Chem. A* **2014**, *2*, 7229−7237.
(36) Kim, J.; Cote, L. J.; Kim, F.; Yuan, W.; Shull, K. R.; Huang, J. Graphene Oxide Sheets at Interfaces. *J. Am. Chem. Soc.* **2010**, *132*, 8180−8186.
(37) Kim, F.; Cote, L. J.; Huang, J. Graphene Oxide: Surface Activity and Two-Dimensional Assembly. *Adv. Mater.* **2010**, *22*, 1954−1958.
(38) Kim, J.; Cote, L. J.; Huang, J. X. Two-Dimensional Soft Material: New Faces of Graphene Oxide. *Acc. Chem. Res.* **2012**, *45*, 1356−1364.
(39) Ye, S.; Feng, J.; Wu, P. Deposition of Three-Dimensional Graphene Aerogel on Nickel Foam as a Binder-Free Supercapacitor Electrode. *ACS Appl. Mater. Interfaces* **2013**, *5*, 7122−7129.
(40) Qiu, L.; Yang, X.; Gou, X.; Yang, W.; Ma, Z. F.; Wallace, G. G.; Li, D. Dispersing Carbon Nanotubes with Graphene Oxide in Water and Synergistic Effects Between Graphene Derivatives. *Chem.—Eur. J.* **2010**, *16*, 10653−10658.
(41) Zhang, C.; Ren, L.; Wang, X.; Liu, T. Graphene Oxide-Assisted Dispersion of Pristine Multiwalled Carbon Nanotubes in Aqueous Media. *J. Phys. Chem. C* **2010**, *114*, 11435−11440.
(42) Tian, L.; Meziani, M. J.; Lu, F.; Kong, C. Y.; Cao, L.; Thorne, T. J.; Sun, Y.-P. Graphene Oxides for Homogeneous Dispersion of Carbon Nanotubes. *ACS Appl. Mater. Interfaces* **2010**, *2*, 3217−3222.
(43) Niu, Z.; Liu, L.; Zhang, L.; Shao, Q.; Zhou, W.; Chen, X.; Xie, S. A Universal Strategy to Prepare Functional Porous Graphene Hybrid Architectures. *Adv. Mater.* **2014**, DOI: 10.1002/adma.201400143.
(44) Zhang, J.; Zhao, X. Conducting Polymers Directly Coated on Reduced Graphene Oxide Sheets as High-Performance Supercapacitor Electrodes. *J. Phys. Chem. C* **2012**, *116*, 5420−5426.
(45) Yang, X.; Zhu, Z.; Dai, T.; Lu, Y. Facile Fabrication of Functional Polypyrrole Nanotubes via a Reactive Self-Degraded Template. *Macromol. Rapid Commun.* **2005**, *26*, 1736−1740.
(46) Ma, Y.; Jiang, S.; Jian, G.; Tao, H.; Yu, L.; Wang, X.; Wang, X.; Zhu, J.; Hu, Z.; Chen, Y. CN_x Nanofibers Converted From Polypyrrole Nanowires as Platinum Support for Methanol Oxidation. *Energy Environ. Sci.* **2009**, *2*, 224−229.
(47) Zhang, X.; Zhang, J.; Song, W.; Liu, Z. Controllable Synthesis of Conducting Polypyrrole Nanostructures. *J. Phys. Chem. B* **2006**, *110*, 1158−1165.
(48) Chen, L.-F.; Zhang, X.-D.; Liang, H.-W.; Kong, M.; Guan, Q.-F.; Chen, P.; Wu, Z.-Y.; Yu, S.-H. Synthesis of Nitrogen-Doped Porous Carbon Nanofibers as an Efficient Electrode Material for Supercapacitors. *ACS Nano* **2012**, *6*, 7092−7102.
(49) Zhang, F.; Xiao, F.; Dong, Z. H.; Shi, W. Synthesis of Polypyrrole Wrapped Graphene Hydrogels Composites as Supercapacitor Electrodes. *Electrochim. Acta* **2013**, *114*, 125−132.
(50) Zhang, L.; Shi, G. Preparation of Highly Conductive Graphene Hydrogels for Fabricating Supercapacitors With High Rate Capability. *J. Phys. Chem. C* **2011**, *115*, 17206−17212.
(51) Lee, M.-S.; Lee, K.; Kim, S.-Y.; Lee, H.; Park, J.; Choi, K.-H.; Kim, H. K.; Kim, D.-G.; Lee, D.-Y.; Nam, S. High-Performance, Transparent and Stretchable Electrodes using Graphene−Metal Nanowire Hybrid Structures. *Nano Lett.* **2013**, *13*, 2814−2821.
(52) Sun, H.; Cao, L.; Lu, L. Bacteria Promoted Hierarchical Carbon Materials for High-Performance Supercapacitor. *Energy Environ. Sci.* **2012**, *5*, 6206−6213.
(53) Wei, L.; Sevilla, M.; Fuertes, A. B.; Mokaya, R.; Yushin, G. Polypyrrole-Derived Activated Carbons for High-Performance Electrical Double-Layer Capacitors with Ionic Liquid Electrolyte. *Adv. Funct. Mater.* **2012**, *22*, 827−834.
(54) Zhang, L. L.; Zhao, X.; Stoller, M. D.; Zhu, Y.; Ji, H.; Murali, S.; Wu, Y.; Perales, S.; Clevenger, B.; Ruoff, R. S. Highly Conductive and Porous ActivatedReduced Graphene Oxide Films for High-Power Supercapacitors. *Nano Lett.* **2012**, *12*, 1806−1812.
(55) Zhu, Y.; Ji, X.; Pan, C.; Sun, Q.; Song, W.; Fang, L.; Chen, Q.; Banks, C. E. A Carbon Quantum Dot Decorated RuO_2 Network: Outstanding Supercapacitances under Ultrafast Charge and Discharge. *Energy Environ. Sci.* **2013**, *6*, 3665−3675.
(56) Yang, M.; Cheng, B.; Song, H.; Chen, X. Preparation and Electrochemical Performance of Polyaniline-Based Carbon Nanotubes as Electrode Material for Supercapacitor. *Electrochim. Acta* **2010**, *55*, 7021−7027.
(57) Song, Y.; Zhou, D.; Wang, Y.; Wang, C.; Xia, Y. Preparation of Nitrogen-Containing Mesoporous Carbons and Their Application in Supercapacitors. *New J. Chem.* **2013**, *37*, 1768−1775.